Superconductor Science and Technology

PAPER • OPEN ACCESS

Elastic-plastic conductor damage evaluation at over 0.4% strain using a high-stress REBCO coil

To cite this article: Jeseok Bang *et al* 2024 *Supercond. Sci. Technol.* **37** 095011

View the article online for updates and enhancements.

You may also like

- Effect of annealing time and pressure on electrical activation and surface morphology of Mg-implanted GaN annealed at 1300 °C in ultra-high-pressure nitrogen ambient
Kensuke Sumida, Kazufumi Hirukawa, Hideki Sakurai et al.
- A new model of fluid flow to determine pressure balance characteristics
P Wongthep, T Rabault, R Noguera et al.
- Comparison of critical current density in SiC-doped *in situ* MgB_2 coils and straight wire samples processed by HIP
D Gajda, A Morawski, A Zaleski et al.

This content was downloaded from IP address 146.201.201.111 on 04/09/2024 at 20:05

OPEN ACCESS
IOP Publishing
Superconductor Science and Technology
Supercond. Sci. Technol. **37** (2024) 095011 (8pp)
https://doi.org/10.1088/1361-6668/ad6a9d

Elastic-plastic conductor damage evaluation at over 0.4% strain using a high-stress REBCO coil

Jeseok Bang*, Griffin Bradford, Kwangmin Kim, Jonathan Lee, Anatolii Polyanskii and David Larbalestier

National High Magnetic Field Laboratory, Florida State University, Tallahassee, FL 32310, United States of America

E-mail: jbang@asc.magnet.fsu.edu

Received 30 April 2024, revised 24 July 2024
Accepted for publication 2 August 2024
Published 12 August 2024

Abstract

Recent reports on screening current stress simulations of high-field REBCO magnets frequently present peak stresses over 1 GPa. However, this result is probably an unrealistic artifact of purely elastic calculations, considering the macroscopic yield and fracture stresses of approximately 900 MPa and less than 1.1 GPa for Hastelloy substrate-coated conductors. Here, we evaluate elastic-plastic conductor damage at over 0.4% strain using a high-stress REBCO coil exposed to a high field to explore this elastic-plastic regime. The coil was located off-center in a low-temperature superconductor magnet so as to induce a significant screening current in the enhanced radial field. Voltage taps, a Hall sensor, and two strain gauges were used for the instrumentation. We obtained strains exceeding 0.4% near the outward edge during the coil current charge from 350 A to 390 A, where the coil was exposed to external axial and radial magnetic fields of 13 T and 0.5 T. *Post mortem* results showed wavy plastic deformation, electrical damage, and REBCO defects. An elastic-plastic simulation reproduced the measured strains and predicted that ∼1 GPa stress is sufficient to induce ∼0.9% strain, thus validating our initial concerns with purely elastic models. This paper provides our experimental and simulation results.

Keywords: screening current, elastic-plastic deformation, high-field and high-stress REBCO magnet, conductor damage, screening current stress, elastoplastic simulation

1. Introduction

Screening current of REBCO-coated conductor amplifies local Lorentz forces by causing a significantly non-uniform current distribution, mostly concentrated on the conductor edges. This distinct nature differentiates the electromagnetic force distribution of REBCO magnets from the conventional electromagnetic force distribution of a magnet that assumes a uniform current distribution and the subsequent magnetic field induction. Indeed, this significant non-uniform current distribution in a high field condition and the subsequent excessively amplified Lorentz force can contribute to excessive hoop tensile stresses, leading to partially, even entirely, irreversible damage to REBCO-coated conductors. Hence, screening current computation has become an essential factor in designing and analyzing high-field REBCO magnets since Hahn *et al* first reported plastic conductor damage caused by screening current stress (SCS) [1]. Naturally, researchers have endeavored to understand this phenomenon, leading to numerous studies, particularly from a numerical perspective [2–7].

* Author to whom any correspondence should be addressed.

Original Content from this work may be used under the terms of the Creative Commons Attribution 4.0 licence. Any further distribution of this work must maintain attribution to the author(s) and the title of the work, journal citation and DOI.

© 2024 The Author(s). Published by IOP Publishing Ltd

Relevant research has shown that SCS can lead to excessive magnetic stresses on REBCO-coated conductors in high-field environments, potentially causing damage to the conductor when the induced strain exceeds 0.4% which is about the 95% critical current (I_c) retention strain [8]. Such SCS-enhanced damage implies that SCS could determine the upper limit of REBCO magnet performance. Hence, many numerical studies of screening current strains have recently been conducted on SCS simulations for high-field REBCO magnets [9–14].

One issue to note is that many such SCS simulations generate GPa-level peak stresses. Such stresses are of real concern since the macroscopic yield stresses of REBCO-coated conductors are approximately 900 MPa, and the fracture stress is less than 1.1 GPa [15]. To address this concern of GPa-level SCS, we revisited the measurement and *post mortem* results related to plastic damage. We have concluded that the conventional simulation, which only considers elastic behavior of REBCO-coated conductors, is insufficient to predict the real behavior of high-field and high-stress REBCO magnets.

This paper provides the design, fabrication, test, and *post mortem* results of a high-stress coil that operated in the cold bore of a low-temperature superconductor (LTS) background magnet. The coil was located off-center in an LTS magnet to generate screening currents. Two strain gauges, located 1 mm away from each edge of the outermost turn, were used for the high-stress evaluation. As a result, we obtained the peak strain of 0.45% (corresponding to 800 MPa) at the sensor location 1 mm away from the top edge when the coil was exposed to external axial and radial magnetic fields of 13 T and 0.5 T and then charged up to 390 A. The measurement implicitly assumed higher stress distribution between the top edge and the sensor location, thus predicting plastic damage at the top edge. Indeed, *post mortem* results showed wavy plastic deformation, electrical damage, and REBCO defects near the top edge of every turn. Elastic and elastic-plastic simulations both reproduced the measured strains at the sensor locations. However, we confirmed that the elastic-plastic simulation predicted the peak stress of ∼1 GPa and explained the *post mortem* results of conductor damage, while the elastic simulation still predicted over 1.1 GPa peak stress.

2. Methods: design and simulation of a no-insulation (NI) REBCO small test coil to be plastically deformed by excessive SCS in a high field

2.1. High-stress REBCO test coil design and experiment setup

The test coil consisting of 20 turns of REBCO-coated conductor was made with the NI winding technique [16]. We used a 3-m long single-slit REBCO-coated conductor whose slit edge faced a background field center. During the coil winding process, weak tension of less than one-kilogram-force was chosen to prevent unnecessary winding damage. Table 1 summarizes the key parameters of the coil.

Table 1. Key parameters of high-stress REBCO test coil.

Parameters		
Conductor		
Manufacturer		SuperPower (SCS4030-AP)
Substrate thickness	[um]	30 (Hastelloy C-276)
Conductor thickness	[um]	45
Conductor width	[mm]	4.00
Critical electric field	[μV cm^{-1}]	1
REBCO coil		
Inner and outer radii	[mm]	19.5; 20.4
Total turns		20
Total length	[m]	2.51
Self-inductance	[μH]	29.95
Operating current	[A]	390
Operating temperature	[K]	4.2 (LHe)
Coil constant	[mT/A]	0.627
Coil critical current (at 1μV cm^{-1})	[A]	700 (SCS not considered)
Coil critical voltage (at 1μV cm^{-1})	[μV]	251
LTS magnet		
Background field	[T]	$(B_z,B_r) = (13,0.5)$
Background magnet constant	[mT/A]	165

The coil location in the cold bore of a LTS magnet was chosen to generate significant SCSs. For substantial induction of screening currents, the bottom surface of the coil is 46 mm away from the center plane of the LTS magnet, where the coil is exposed to external axial and radial fields of 13 T and 0.5 T. Measurement results of the field-dependent I_c information of the REBCO-coated conductor used for this coil fabrication estimated a conductor I_c of 700 A at the external axial and radial fields of 13 T and 0.5 T and at 4.2 K. Therefore, we were able to assume a coil I_c of 700 A if additional dependencies on I_c, e.g. strain-dependent I_c degradation caused by SCS, were not considered.

We attached two strain gauges (commercial products) to the outermost turn in the coil to measure local strains. Each strain gauge was calibrated by multiple uniaxial stress tests at low temperatures of 77 K and 4.2 K and could measure at most 1% strain with a resolution of 0.002%. Their centers were located 1 mm away from each edge (the sensor width is almost 2 mm), so they cannot measure the peak elastic-plastic strains that cause plastic waviness of the outward top edge. The coil was also instrumented to measure voltage and the axial magnetic field at the coil center. Figure 1 presents a schematic of the experiment and a photo of the test coil.

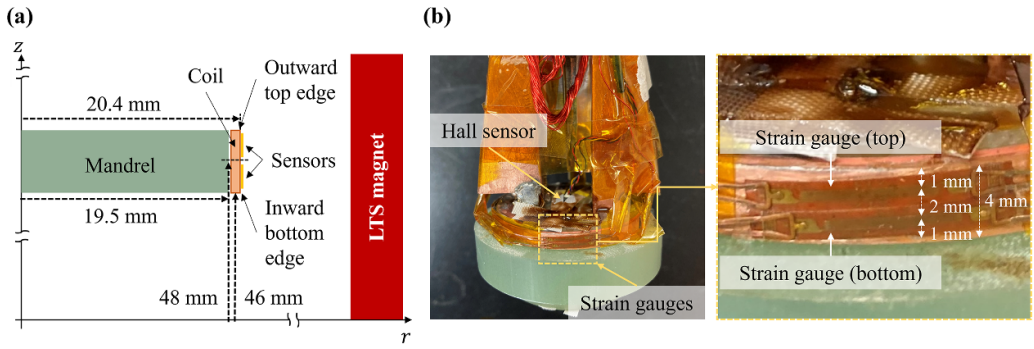

Figure 1. Experimental setup: (a) a schematic drawing and (b) a photo of the high-stress REBCO test coil with strain gauges attached.

2.2. SCS-enhanced elastic-plastic conductor deformation simulation

We used a multiphysics finite element modeling technique to simulate SCS-enhanced elastic-plastic conductor deformation. Two physics, electromagnetics and mechanics, were coupled for this modeling. Details of each simulation are described below.

For electromagnetic simulation, the H-formulation using edge elements was set to be the governing equation [17]. A homogenized domain and the corresponding weak integral constraint of current were used to improve computational speed without loss of calculation accuracy [18]. Two fundamental circuit laws, i.e. Kirchhoff's current and voltage laws, were used to compute radial (transverse) and azimuthal (longitudinal) currents in an NI coil; we assumed no axial component of current densities. The time derivative of the radial magnetic field was set to be an additional source term to consider current induction by external fields. Dirichlet boundary condition of zero fields at a closed boundary far from the current source (so-called the 'air' boundary) was used to complete this electromagnetics modeling. The power-law $E-J$ model was set to be the material property defining the $V-I$ behavior of the coated conductors [19]. Further settings of this simulation method are described in our previous works [20–26].

For mechanical simulation, the force/momentum balance equation was set to be the governing equation. The calculated Lorentz forces from the electromagnetic simulation were assigned as the body load. Here, we assumed zero axial displacements at the coil bottom surface, considering the coil test condition using a cryogenic probe (figure 1). Therefore, the roller boundary condition was assigned only at the bottom surface. It was also assumed that the dry-winding configuration of the test coil resulted in turn-to-turn contacts between individual turns. Accordingly, the contact boundary condition at every contact surface was considered a boundary condition. Two turns are regarded as one engineering turn to ease the computational cost [11, 12]. Since our *realistic* elastic-plastic deformation simulation required the measured mechanical characteristics of the conductor used for this test coil, we measured Young's modulus of the REBCO-coated conductor using a uniaxial tensile test (figure 2). The measured stress–strain curve (the black line with symbols) was modeled into

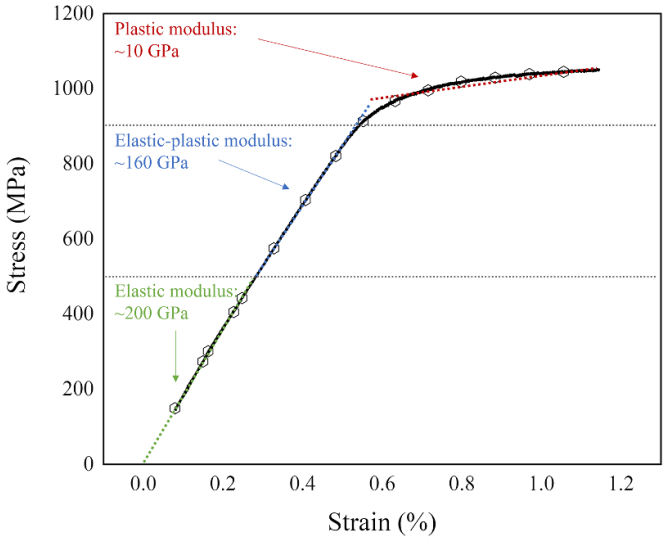

Figure 2. The measured uniaxial stress–strain curve of the REBCO-coated conductor type used in our coil.

pure elastic (the green line), Hastelloy-elastic-Copper-plastic (the blue line), and pure plastic (the red line) regimes.

This simulation work did not consider the local heat-dissipative behavior and the subsequent temperature change. Indeed, the measured peak instantaneous heat dissipation of the test coil was 0.2 W during the test, so we were able to assume a marginal temperature increase if considering the liquid helium environment. Thus, we set a constant operating temperature of 4.2 K in this simulation work.

Lastly, we should note that conventional SCS simulations generally consider the pure elastic line (rarely, the pure elastic and Hastelloy-elastic-Copper-plastic lines). Due to this consideration, calculated stresses can increase continuously, even beyond 1 GPa, as proportional to strains and elastic Young's modulus. However, plastic deformation occurs in reality, thus notably reducing the effective modulus when stresses exceed the elastic threshold. Hence, we considered the tangent modulus measured in each deformation regime and the macroscopic initial yield stress of about 900 MPa in the elastic-plastic simulation. This elastic-plastic simulation attempt was made earlier [27–29] but has not been validated with strain gauges or displacement measurements.

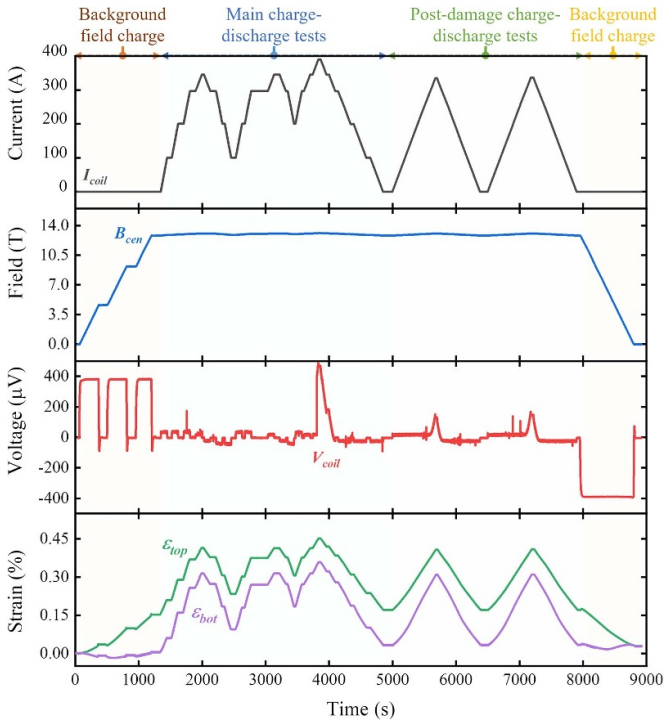

Figure 3. Measurement results of the coil current, coil voltage, coil center field, and strains. Note that strain gauges were located 1 mm away from each edge, so we could not have measured strains at the top edge, where the highest strain is expected.

3. Results: elastic-plastic conductor damage evaluation

3.1. Over 0.4% strain operation at axial and radial fields of 13 T and 0.5 T

The background field was energized first, then the test coil was charged. The coil current ramp rate was set to be 0.1 A/s below 300 A but 0.05 A/s above 300 A. Several repeated charge and discharge steps were utilized to confirm data reproducibility. Figure 3 summarizes the measured current, voltage, field, and strain during the test.

During the background field charge (0–1300 s in figure 3), the measured strain at 1 mm away from the outward top edge (ϵ_{top}) increased proportionally to the field intensity. Note that the polarity of screening currents induced by the radial field penetrating individual winding turns is opposite at the top and bottom edges. Indeed, ϵ_{top} was always positive, but ϵ_{bot} was always negative. The peak ϵ_{top} was 0.15% when the background field was fully charged and correspondingly exposed axial and radial magnetic fields of 13 T and 0.5 T to the coil, where ϵ_{bottom} was −0.00%. The peak ϵ_{bot} was −0.02% when the axial and radial fields were 6 T and 0.2 T. An intriguing observation was the notable strain increase in ϵ_{top}, unlike ϵ_{bot}. The pure SCSs (no transport current) caused tensile hoop stresses at the top edge. In this situation, the dry-winding configuration allowed each turn to move outward away from the winding bobbin by enabling turn-to-turn separation, and accordingly, ϵ_{top} was able to increase quickly. In contrast, compressive hoop stresses at the bottom edge by pure SCSs barely affected ϵ_{bot} since there was little space for each turn to move inward towards the winding bobbin due to the compact NI dry-winding pack.

During the first charge–discharge step (1300–2500 s in figure 3), we obtained ϵ_{top} of 0.42% and ϵ_{bot} of 0.32% at 345 A. No observed electrical damage and corresponding I_c degradation appeared, and the reproducibility was confirmed by the second charge–discharge step (2500–3500 s). However, a voltage jump of 360 μV appeared on reaching 380 A during the third charge–discharge step (3500–5000 s). ϵ_{top} and ϵ_{bot} were 0.44% and 0.34% at 380 A. We interpreted this voltage spike as indicating that electrical damage occurred first at the outermost turn where turn-to-turn contact is absent [30]. We also concluded that the coil operating current exceeded the coil I_c since the coil voltage exceeded the coil critical voltage of 251 μV at an electric field of 1 μV cm^{-1}.

Despite the damage, the coil was charged 10 A higher to investigate dissipative flux-flow behavior. At the peak current of 390 A, the measured voltage was 470 μV, and peak strains were $\epsilon_{top} = 0.45\%$ and $\epsilon_{bot} = 0.35\%$. During the discharge from 390 A to 0 A, we observed the voltage difference of 180 μV at 345 A by comparing coil voltages before and after the 0.45% operation, which we attribute to I_c degradation by SCS. This coil voltage comparison led us to conclude permanent electrical damage. We additionally measured the flux-flow voltage of 130 μV at 335 A twice during the sequential charge–discharge steps after the 0.45% strain operation (5000–8000 s in figure 3), a result well consistent with the measured voltage at the same current during the discharge from 390 A to 0 A. Figure 4 compares coil voltages before and after the 0.45% strain operation and summarizes key measurements that lead us to conclude that we observed I_c degradation by SCS.

Further voltage analysis confirmed a change of the coil I_c after these cycles. The power-law $E-J$ model was used to calculate I_c at the lumped circuit model perspective, where we assumed a constant index value of 30 and a critical electric field of 1 μV cm^{-1}; this approach is conventionally used to estimate coil I_c. The measured coil voltages were 466 μV at 390 A, 180 μV at 345 A, and 130 μV at 335 A, from which we estimated the coil I_c as 382, 348, and 342 A at 390, 345, and 335 A, respectively. Though the coil I_c was marginally different between 345A and 335A, the notable difference between 390A and 345A was probably attributed to the following mechanism. The damage occurred first at 380A and further increased while raising the coil current to 390 A, which drove increasing tensile hoop stress by SCS. However, the damage became even more severe during the current discharge from 390A to 345A.

3.2. Elastic-plastic conductor damage inspection

We carefully unwound the coil to inspect for visible mechanical damage. During unwinding, we observed wavy plastic

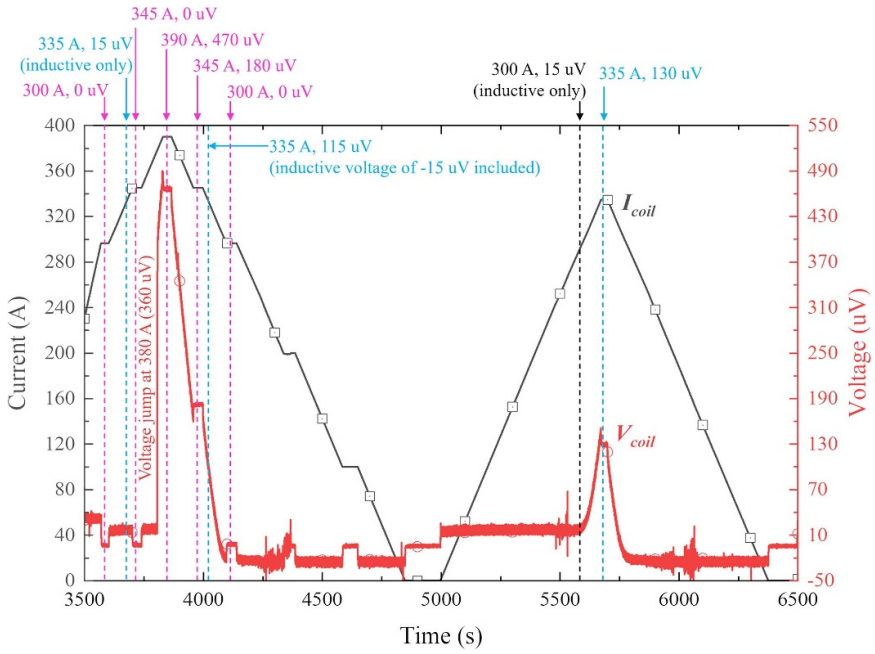

Figure 4. Observation of I_c degradation. This figure compares measured voltages before and after 0.45% strain operation.

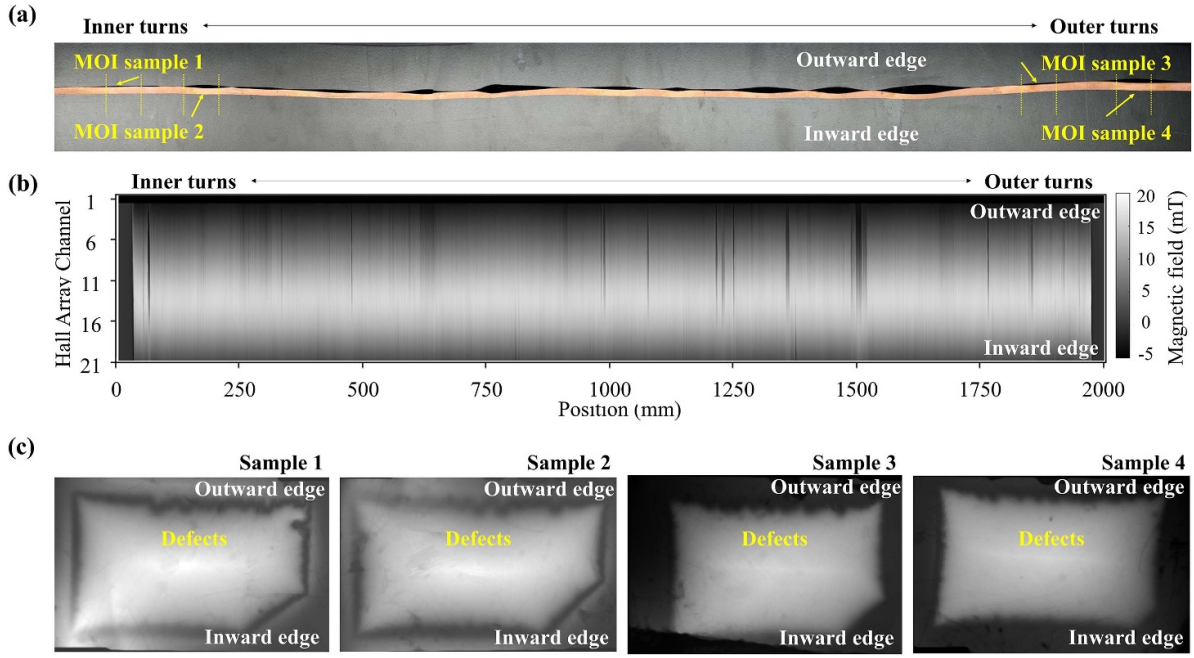

Figure 5. *Post mortem* results: (a) coil-unwinding results showing wavy plastic damage at the outward edge of the REBCO-coated conductor, and (b) and (c) YateStar and MOI inspection results to investigate electromagnetic damage.

deformation in every turn, but it appeared only at the outward edge (figure 5(a)). This observation leads us to conclude elastic deformation at the inward edge with only marginal electrical damage. The period of waviness was mostly constant at about one turn length (about 12 cm) while sometimes half [11]. Most of the edge wave's nodes produced by the plastic deformation were radially aligned at the same angle along the line connecting solder points at the inlet and outlet current leads soldered to the innermost and outermost turns.

YateStar [31], a continuous lengthwise transverse I_c uniformity measuring tool, measures the local magnetization of REBCO-coated conductors that pass through a 0.5 T quadrupole magnet (figure 5(b)). YateStar inspection results showed periodic electrical damage which illustrate that the damage started from the outward top edge. Permanent

electrical damage of the conductor was evaluated by the relative I_c transformed from the measured magnetization results. The evaluation showed that the waviness caused by SCS caused about ∼20% of the I_c dropout. Additionally, YateStar analyzed the period of electrical damage as one-turn length using a Fourier analysis of measured uniformity, a result consistent with the observed unwinding result.

Magneto-optical imaging (MOI) can evaluate sensitively at the scale of ∼10 μm the uniformity of supercurrent flow under fields up to ∼0.1 T [32]. Four samples were inspected, two from the innermost turn of the coil and two from the outermost turn. MOI inspection results compared the defects at the outward and inward edges (figure 5(c)). This local magnetization study by MOI showed that plastic damage caused REBCO defects but only concentrated on the outward edge where the highest SCS was predicted. However, we did not observe magnetic field penetration by current-flow blocking defects across the conductor except around the wavy damage regions. This finding indicated that elastic deformation was predominant during the experiment.

4. Discussion: elastic-plastic conductor damage analysis

We analyzed the observed conductor damage using the in-house simulation model described in the Methods section. Two SCS simulations were conducted: one with screening current and elastic deformation simulations (conventional) and the other with screening current and elastic-plastic deformation simulations. For the first, the pure elastic modulus of 200 GPa was set to be the mechanical deformation property, while the second considered the measured elastic-plastic stress–strain curve. Figure 6 summarizes simulation results of strains at the strain gauges locations (figure 1); note that the center of the sensors was located 1 mm away from each edge. In addition, this figure compares simulation results of the hoop stress σ_{hoop}, hoop strain ϵ_{hoop}, and elastic-plastic deformation distributions at the peak current of 390 A. Simulated total displacements at the peak current are also displayed in the cross-sectional view of the coil.

The conventional elastic simulation results of strains at the strain gauge locations show reasonable agreement with measurements. However, the simulation still predicts excessive stress of >1.1 GPa at the peak current of 390 A, inconsistent with the *post mortem* results. In addition, the key deficiency of the conventional simulation is that it cannot explain how plastic damage is distributed within the coil and how I_c degradation happens. Nevertheless, an intriguing comparison is that the elastic simulation can reproduce the measured strain at the inward bottom edge, a result consistent with the conclusion from *post mortem* results that only elastic deformation occurred at the bottom edge, unlike the elastic-plastic deformation at the top edge.

However, we were able to simulate the observed SCS-induced conductor damage more precisely by considering the measured elastic-plastic stress–strain curve. The elastic-plastic simulation reproduced the measured strains better than the elastic simulation and even offered a plastic deformation distribution within the coil, consistent with the *post mortem* results. The simulation results demonstrate that elastic-plastic conductor damage occurs at the top edge but is predominantly elastic elsewhere. In addition, this simulation study provides three conclusions. First, the simulation results at the peak current of 390A demonstrate that excessive SCS beyond the initial yield strength of 900 MPa should have caused wavy plastic deformation and permanent electrical damage at the top edge. Second, elastic-plastic analysis of the conductor confirms that ∼0.9% strain could have occurred at ∼1 GPa, which clarifies that over 1 GPa SCS in the high-field and high-stress REBCO magnet design and analysis is unrealistic. Lastly, SCS analysis results show that ∼60% of each turn experienced 600 MPa (initial I_c degradation stress) [8], consistent with the measured ∼50% coil I_c degradation by SCS (table 1 and figure 4).

In addition, our simulation of elastic-plastic deformation explained the reason for the observed wavy damage and evaluated the effect of SCS-enhanced radial stresses on conductor damage. First, figure 6(b) shows plastic damage concentrated at the top edge of every turn. Indeed, our elastic-plastic simulation computed residual deformation caused by elastic-plastic damage across the conductor width, expected after the high-stress test ended. We found that the computed residual deformation is maximum at the top edge of the outermost turn as 18 μm, continuously decreases towards the bottom edge, and becomes 0 μm (no deformation) at the middle of the conductor. There was no deformation between the middle and the bottom edge. This finding, consistent with our *post mortem*, explained that tensile hoop stress by SCS caused irreversible circumferential length increment at the top edges, thus resulting in wavy damage. Next, our SCS simulation showed that the peak radial stresses are much smaller than the peak hoop stresses at 390 A, leading to the conclusion that the observed conductor damage was mainly caused by excess tensile hoop stress. Indeed, our *post mortem* did not find any aftereffects related to excess radial stresses, e.g. internal delamination between Hastelloy substrate and REBCO layers. Detailed voltage analysis complemented this conclusion further. If the coated conductor had layer-to-layer internal delamination, the resistive voltage behavior should have been continuously observed. However, as shown in measurement results during post-damage charge–discharge tests, there was no resistive voltage increase. Accordingly, we were able to explain that excess tensile hoop stresses caused outward edge cracks and their propagation as inspected by the local magnetization study, and these defects would have degraded the coil I_c.

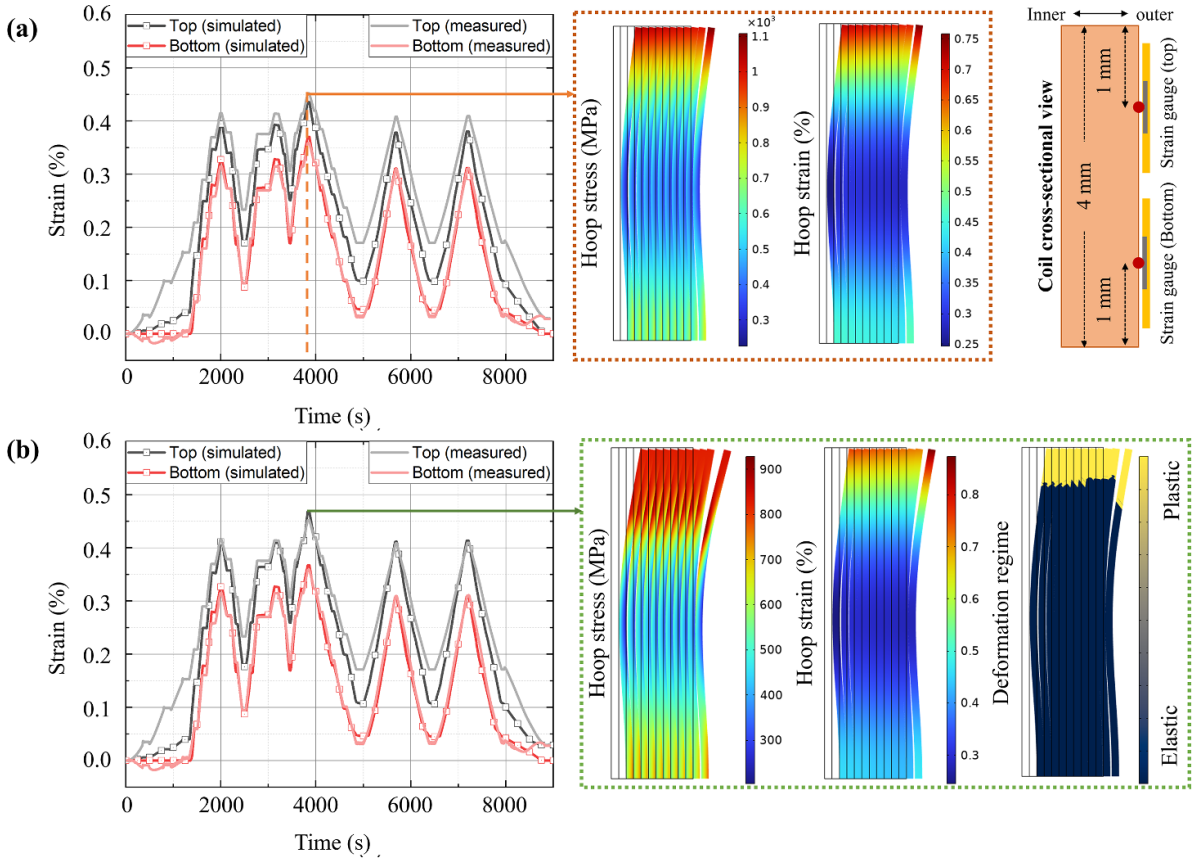

Figure 6. SCS simulation results: (a) elastic simulation, (b) elastic-plastic simulation. This figure compares the simulation and measurement results of strains measured at the locations away 1 mm from the top and bottom edges over the test. In boxes, simulated hoop stress σ_{hoop}, hoop strain ϵ_{hoop}, elastic-plastic deformation, and total displacement distributions at 390 A are displayed.

Interestingly, this study revisits our previous observation of two undamaged coils in the third coil of the 'Little Big Coil' test campaign (LBC3) that explored 45.5 T [1]. The undamaged coils were the second and eleventh coils in a stack of twelve coils. Unlike other coils, they were wound using single-slit conductors and their slit edges pointed inward toward the background field center, the same configuration as the high-stress coil tested here. Our measurement and our elastic-plastic simulations conclude that the undamaged coils did experience less than 900 MPa, leading us to a notable discrepancy with simulated elastic-only peak stress of >1.2 GPa [11].

5. Conclusion

This paper evaluated elastic-plastic conductor damage at over 0.4% strain using a high-stress REBCO coil that was charged up to 390 A while exposed to external axial and radial fields of 13 T and 0.5 T. *Post mortem* results showed elastic-plastic conductor damage. Experimental and *post mortem* results were analyzed by an electromagnetic-mechanical simulation that includes screening current and elastic-plastic simulations. The simulation reproduced the measured strains and explained observations of plastic wavy deformation, permanent electrical damage, and I_c degradation by SCS. Through this study, we confirmed the importance of considering the elastic-plastic behavior of a REBCO-coated conductor in understanding SCS and conductor damage.

Data availability statement

All data that support the findings of this study are included within the article (and any supplementary files).

Acknowledgments

A portion of this work was performed at the National High Magnetic Field Laboratory, which is supported by the National Science Foundation Cooperative Agreement No. DMR-2128556 and the State of Florida. This work is also supported by the Office of Fusion Energy Sciences Grant DE-SC0022011.

ORCID iDs

Jeseok Bang https://orcid.org/0000-0002-4761-6334
Griffin Bradford https://orcid.org/0000-0003-3847-8213
Anatolii Polyanskii https://orcid.org/0000-0002-5977-5324
David Larbalestier https://orcid.org/0000-0001-7098-7208

References

[1] Hahn S *et al* 2019 *Nature* **570** 496–9
[2] Li Y, Park D, Lee W, Choi Y, Tanaka H, Bascuñàn J and Iwasa Y 2020 *IEEE Trans. Appl. Supercond.* **30** 4702305
[3] Takahashi S, Suetomi Y, Takao T, Yanagisawa Y, Maeda H, Takeda Y and Shimoyama J I 2020 *IEEE Trans. Appl. Supercond.* **30** 4602607
[4] Yan Y, Xin C, Guan M, Liu H, Tan Y and Qu T 2020 *Supercond. Sci. Technol.* **33** 05LT02
[5] Yan Y, Song P, Xin C, Guan M, Li Y, Liu H and Qu T 2021 *Supercond. Sci. Technol.* **34** 085012
[6] Xia J, Bai H, Yong H, Weijers H W, Painter T A and Bird M D 2019 *Supercond. Sci. Technol.* **32** 095005
[7] Ueda H, Maeda H, Suetomi Y and Yanagisawa Y 2022 *Supercond. Sci. Technol.* **35** 054001
[8] Barth C, Mondonico G and Senatore C 2015 *Supercond. Sci. Technol.* **28** 045011
[9] Kolb-Bond D, Bird M, Dixon I, Painter T, Lu J, Kim K, Kim K, Walsh R and Grilli F 2021 *Supercond. Sci. Technol.* **34** 095004
[10] Yan Y, Li Y and Qu T 2021 *Supercond. Sci. Technol.* **35** 014003
[11] Hu X *et al* 2020 *Supercond. Sci. Technol.* **33** 095012
[12] Park J, Bang J, Bong U, Kim J, Abraimov D and Hahn S 2021 *IEEE Trans. Appl. Supercond.* **31** 4603205
[13] Ueda H, Awazu Y, Tokunaga K and Kim S 2021 *Supercond. Sci. Technol.* **34** 024003
[14] Suetomi Y, Xu P, Bosque E S, Gavrilin A V, Markiewicz W D, Bai H and Dixon I R 2023 *IEEE Trans. Appl. Supercond.* **34** 8400206
[15] Zhang Y, Hazelton D, Kelley R, Kasahara M, Nakasaki R, Sakamoto H and Polyanskii A 2016 *IEEE Trans. Appl. Supercond.* **26** 8400406
[16] Hahn S, Park D K, Bascunan J and Iwasa Y 2010 *IEEE Trans. Appl. Supercond.* **21** 1592–5
[17] Brambilla R, Grilli F and Martini L 2006 *Supercond. Sci. Technol.* **20** 16–24
[18] Zermeno V M, Abrahamsen A B, Mijatovic N, Jensen B B and Sørensen M P 2013 *J. Appl. Phys.* **114** 173901
[19] Rhyner J 1993 *Physica* C **212** 292–300
[20] Bang J, Kim S, Jang J Y, Hwang Y J, Cho M, Kim J, Lee J T, Ahn M C, Lee S and Hahn S 2019 *IEEE Trans. Appl. Supercond.* **29** 4601305
[21] Bang J *et al* 2020 *IEEE Trans. Appl. Supercond.* **30** 4901405
[22] Bang J, Kim J, Lee J T, Kim G, Park J, Park S H, Noguchi S and Hahn S 2022 *J. Appl. Phys.* **132** 183911
[23] Bang J, Park S H, Park J, Kim G, Lee J T, Kim K, Hahn S and Larbalestier D C 2022 *IEEE Trans. Appl. Supercond.* **32** 1–5
[24] Bang J, Park J, Choi K, Kim G and Hahn S 2023 *Supercond. Sci. Technol.* **36** 085003
[25] Bang J, Kim K, Bradford G, Lee J, Abraimov D, Mato T, Noguchi s, Hahn s and Larbalestier D 2024 *IEEE Trans. Appl. Supercond.* **34** 4902105
[26] Bang J 2024 *IEEE Trans. Appl. Supercond.* **34** 4904907
[27] Gao P, Chan W K, Wang X, Zhou Y and Schwartz J 2020 *Supercond. Sci. Technol.* **33** 044015
[28] Trillaud F, Berrospe-Juarez E, Zermeño V M and Grilli F 2022 *Supercond. Sci. Technol.* **35** 054002
[29] Yan Y, Park J, Kim J, Bong U, Kim G, Jang W and Hahn S 2024 *IEEE Trans. Appl. Supercond.* **34** 4602605
[30] Matsuda T, Okamura T, Hamada M, Matsumoto S, Ueno T, Piao R, Yanagisawa Y and Maeda H 2018 *Cryogenics* **90** 47–51
[31] Coulter J, Ugurlu O, Willis J, Holesinger T and Xie Y Y 2010 Identifying and Investigating J c Variations in Coated Conductors Fabricated by Mocvd/ibad *AIP Conf. Proc.* **1219** 347–54
[32] Polyanskii A, Emergo R, Wu J, Aytug T, Christen D K, Perkins G and Larbalestier D 2005 *Phys. Rev.* B **72** 174509